Advances in Research

Volume 25, Issue 3, Page 97-112, 2024; Article no.AIR.114757
ISSN: 2348-0394, NLM ID: 101666096

Surface and Subsurface Structural Mapping of Lokoja Central Nigeria Using Airborne Magnetic and Remote Sensing Data

Akpaneno, A. F. [a*] and Tawey, M.D [b]

[a] Department of Geophysics, Federal University Dutsinma, Katsina State, Nigeria.
[b] National Water Resources Institute, Mando Road, Kaduna, Nigeria.

Authors' contributions

This work was carried out in collaboration between both authors. Both authors read and approved the final manuscript.

Article Information

DOI: 10.9734/AIR/2024/v25i31054

Open Peer Review History:
This journal follows the Advanced Open Peer Review policy. Identity of the Reviewers, Editor(s) and additional Reviewers, peer review comments, different versions of the manuscript, comments of the editors, etc are available here: https://www.sdiarticle5.com/review-history/114757

Original Research Article

Received: 21/01/2024
Accepted: 29/03/2024
Published: 02/04/2024

ABSTRACT

The main goal of this research is to evaluate the surface and subsurface structural framework of Lokoja and its surroundings using airborne magnetic and Shuttle Radar Topographic Mission (SRTM) data by applying image processing techniques. To explicate our aim, the residual magnetic intensity (RMI) data was reduced to a magnetic pole (RTP) to centre the anomalies above their causative source after which, the data was subject to the first vertical derivative filter and 3D Euler deconvolution method with structural index (SI =1) where the subsurface structures were delineated, using Oasis Montaj software. Four (4) shaded relief images were created with light sources emanating from four different directions to identify linear terrain features in the SRTM data at a solar azimuth of 0˚ and a solar elevation of 45˚. Others 90˚, and 135˚ followed by creating a composite shaded relief image of all four. The PCI Geomatica edge detection algorithm was applied to the composite shaded relief image produced. After thresholding and filtering processes,

**Corresponding author: E-mail: aniefiokakpaneno@gmail.com;*

structural lineaments were extracted from the edges of the image by subjecting it to the line algorithm of PCI Geomatica. ArcGIS v10.7.1 was used to assign geometry to both magnetic and SRTM structures delineated. The resulting structural lineaments were subjected to Rockworks where a rose diagram that depicts structural trends within the study area was produced. The lineaments delineated allow us to decipher that the area is dissected by numerous subsurface and surface linear structures and these lineaments trend predominantly in the NE-SE, WSW-ENE, NW-SE, and NNE-SSW directions. Overlying the lineaments drawn from the pair of data sets showed several sites of structural coincidence that are thought to be structural continuation locations where subsurface fluids such as water will migrate directly to the surface.

Keywords: Structural lineaments; aeromagnetic; RTP; SRTM; Edge detection; groundwater exploration; geologic structures.

1. INTRODUCTION

Geological structures (surface and subsurface) play a crucial role in groundwater exploration especially in the basement complex as water is hosted within the secondary structures (Faults, joints, and fractures), in dam design, the knowledge of the structural framework of a place provided by geoscientists to the engineers can provide them with a clue on how the dam is to be designed [1,2]. Also, these geologic structures are conduits that allow fluid to flow into host rocks as such, they can host water, oil and ore minerals [3,2]. Two sets of data have been utilized to delineate the surface and subsurface geologic structures within the study area. These are topographic and airborne magnetic data. Hillshade maps produced from Shuttle Radar Topography Mission (SRTM), digital elevation model (DEM) has been used in several published research papers to delineate surface structures which are reflections of subsurface geologic structures [4-7,1,8-13].

Airborne magnetic surveys are a very important first step in geophysical exploration because they make it possible to find ambient magnetic fields produced by subsurface magnetic minerals [14], most of these magnetic minerals are associated with geologic structures as such, airborne magnetic data is the most widely used in the delineation of subsurface geologic structures for minerals [15,16]. Integrating magnetic data and other methods has provided subsurface evidence of mineralisation or associated structures/alteration zones [17,18,19,20]. Works have been published employing airborne magnetic data for structures and mineralization [21,1]. Several other works have also been published employing the integration of airborne magnetic and remote sensing data for structural delineations [22,23,24,25,26].

The goal of the present study is to carry out surface and subsurface structural mapping of Lokaja (sheet 247).

The objectives of the study are to Produce the first vertical derivative and 3D Euler deconvolution maps of the area for subsurface structural delineation, produce a hillshades map of the study area for surface structural delineation carry out statistical structural analysis of the study area and produce a combined structural map showing areas of structural overlap between surface and subsurface structures.

1.1 Location, geology and topography of the study area

The study area is bounded by longitude 6˚ 30′ E to Longitude 7˚ E and Latitude 7˚ 30′ N to Latitude 8˚ N and it is located within southcentral Nigeria, with the Nigeria confluence town (Lokoja), almost at the centre of it (Fig. 1). Tectonically, it is situated within the Togo - Benin - Nigeria swell that is adjacent to the Togo belt, all of which are a product of the Pan African Orogeny and is bordered by the Volta Basin to the west, the Sokoto Basin that is the continuation of Iullemeden Basin in the north, the Chad Basin in the northeast and the Benue trough in the east (Fig. 1). The geology of the area is partly basement to the west and sedimentary to the east. Rocks within this area as displayed on the geologic map of the study area (Fig. 1) are Banded gneiss/Biotite gneiss, Migmatite, Granite Gneiss, Undifferentiated older granite, River Alluvium, Undifferentiated Schist, False bedded sandstone, Coal, sandstone and shale, Mudstone and shale, Feldspathic sandstone and siltstone, Undifferentiated older granite, and Charnockitic Rocks [27]. The topographic variation across the study area ranges from 38 m low to 540 m high, above the main sea level (Fig. 2).

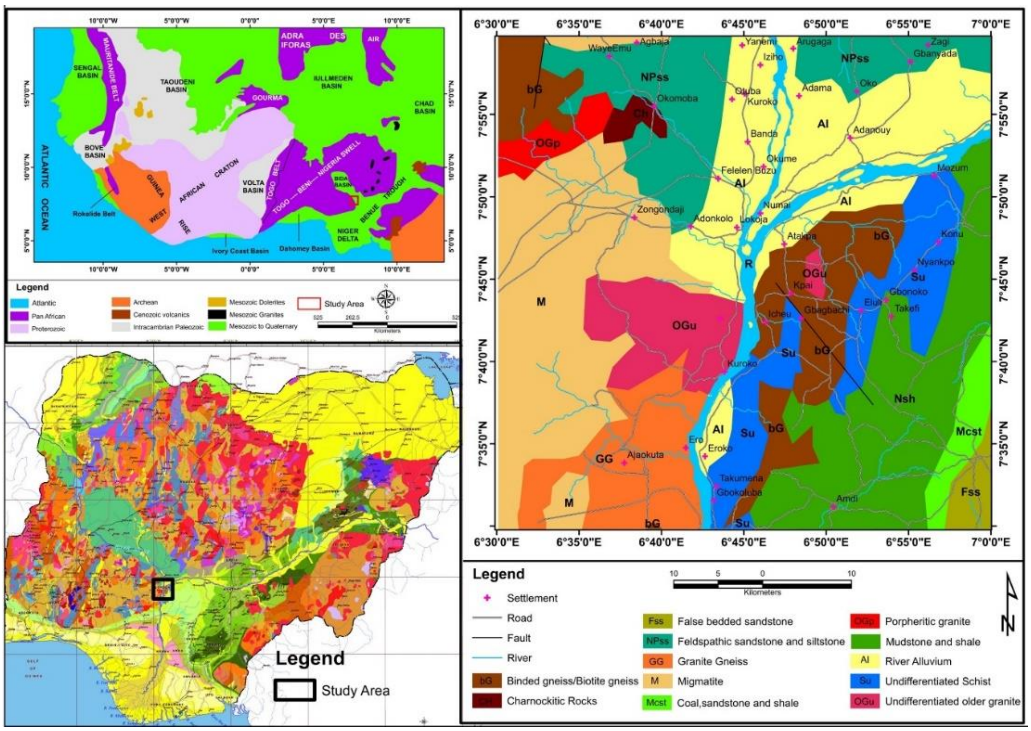

Fig. 1. Location and Geologic map of the study area (modified from NGSA, 2006 and Wright, 1985)

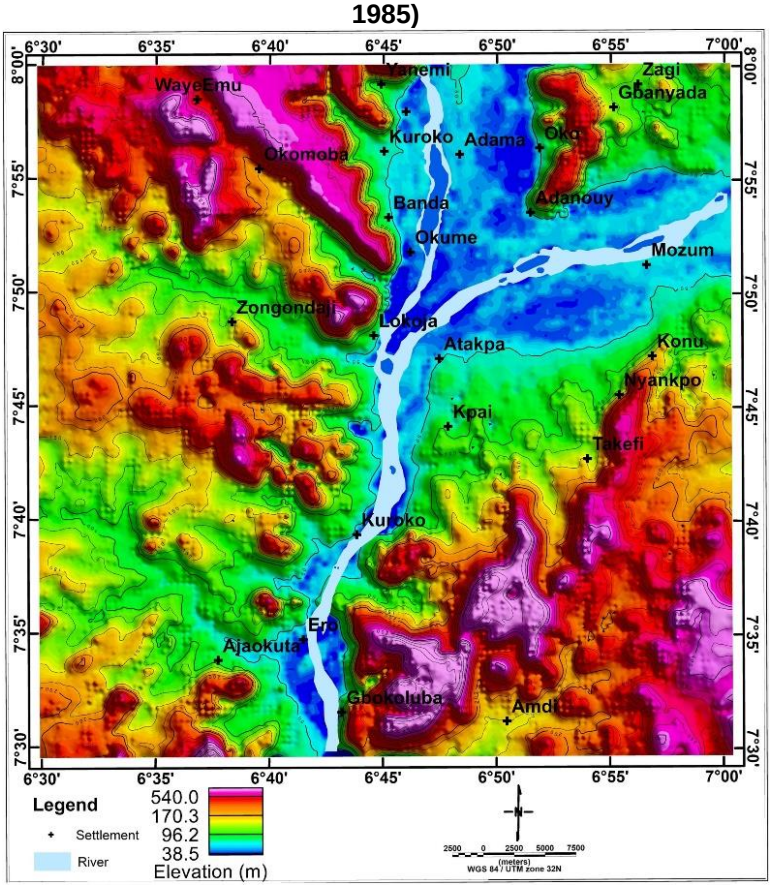

Fig. 2. a. Digital elevation map (DEM) of the study area. Source (Modified from USGS website, *Available:https://earthexplorer.usgs.gov/*

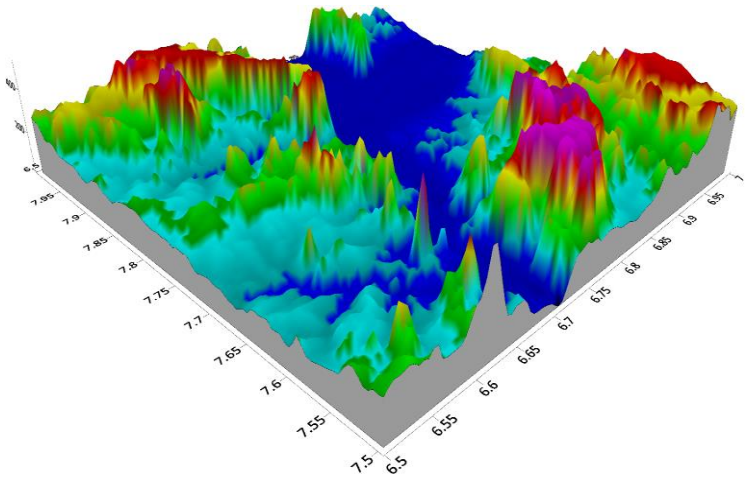

Fig. 3. 3D Digital elevation map (DEM) of the study area

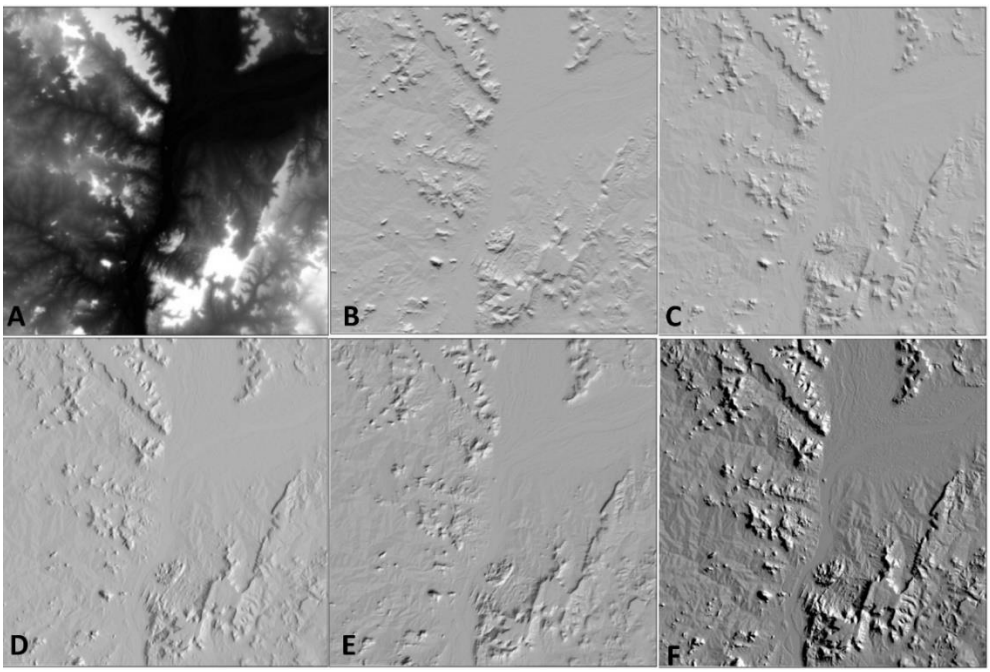

Fig. 4: a. SRTM DEM of the study area with a solar azimuth of b. 0°, c. 45°, d. 90° and 135° hillshade maps and F. the combined hillshade map

2. Materials and Methods

2.1 Sources of Data Magnetic data

The Nigerian Geological Survey Agency (NGSA), Abuja, provided the airborne magnetic data that was utilised in this investigation. The Fugro airborne surveys were responsible for the collection and processing of the data and the data were recorded for magnetic measurements at an interval of 0.1 s (~7.5 m) for magnetic data recording interval, 80 meters for sensor mean terrain clearance, 500 meters for flight lines, 5000 meters for tie lines, 135˚ for flight lines, and 45˚ for tie lines.

2.2 Sources of Remote sensing data

The Digital elevation model (DEM) by the Shuttle Radar Topographic Mission (SRTM) with serial number (n07_e006_1arc_v3.tif) was downloaded from the USGS website (*https://earthexplorer.usgs.gov/*) and has a spatial resolution of 30 m.

2.3 Methodology

The magnetic data was processed using Oasis Montaj software. This was done by first reducing the Residual magnetic intensity data to the pole (RTP) using inclination and declination angle values of (-9.45˚and -2.15˚) with Amplitude inclination correction of -90˚. The first vertical derivative filter was then applied to the RTP for magnetic structural delineation. Also, the RTP data was subjected to Euler deconvolution with a structural index equal to 1 for structural depth and trend delineation. Hillshade maps using four distinct solar azimuths of 0˚, 45˚, 90˚, and 135˚ followed by the creation of a composite shaded relief image that combined the four images produced (Fig. 3). The PCI Geomatica edge detection algorithm was applied to the composite shaded relief image that was produced. After thresholding and filtering processes, structural lineaments were extracted from the edges of the image by subjecting it to the line algorithm of PCI Geomatica. ArcGIS v10.7.1 was used to assign geometry to both magnetic and SRTM structures. The resulting structural lineaments were subjected to Rockworks where a rose diagram that depicts structural trends within the study area was produced for both surface and subsurface structures.

2.4 Theory of the Methods

2.4.1 Reduction to magnetic pole (RTP)

Magnetic anomalies in low and middle latitudes, unlike gravity anomalies, exhibit polarity, confounding interpretation. Magnetic anomalies take on this form due to the inclination of the induced field vector or magnetization vector [28]. Baranov [29] introduced RTP, a transformation operation devised by Bhattacharya [30], which allows for the reorientation of magnetic anomalies above the causal source to counteract this skewness. According to Li [31], RTP is an important effective operation that converts a total magnetic anomaly caused by a source into the anomaly produced by the same source if it was situated at the pole and magnetised solely by induction. When the Earth's field is inclined, induction-based magnetic anomalies have patterns or forms that are unevenly comparable or linked to their sources; when the inducing field is vertical, the induced anomalies are consequently over their sources [32].

The RTP operation in the wavenumber domain can be expressed as:

$$M_p(u,v) = \frac{M_c M_p(u,v)}{[\sin(I)+i\cos(I)\ \cos(D-\Theta)]^2} \quad (1)$$

where:

$M_p(u,v)$ is the Fourier Transform of these observed magnetic data,
$M_c(u,v)$ is the Fourier Transform of the vertical magnetic field,
I and *D* is the inclination and declination of the core field,

(u,v) is the wavenumber corresponding to the (x,y) directions respectively and $\theta = arctan\left(\frac{u}{v}\right)$ (Luo et al. [33].

2.5 Vertical Derivatives

Vertical derivative filters are commonly applied on magnetic grids via fast Fourier transform (FFT) filters. They improve short-wavelength components of the magnetic field [34], which may be accomplished by increasing the field's amplitude spectra by a factor.

$$\frac{1}{n}\left[(U^2+V^2)^{\frac{1}{2}}\right]^n \quad (2)$$

where n is the order of the vertical derivative, and (U, V) is the wavenumber corresponding to the (x, y) directions respectively.

2.6 3D Euler Deconvolution

Reid et al. [35] define Euler deconvolution as a boundary and depth estimator. It retrieves data from grids based on Thompson's [36] homogeneity relationship. This connection may be written in the following way:

$$(x-x_0)\frac{\delta T}{\delta x}+(y-y_0)\frac{\delta T}{\delta y}+(z-z_0)\frac{\delta T}{\delta z}=N(B-T) \quad (3)$$

where $(x_0, y_0\ z_0)$ is the position of a magnetic source whose total field T is detected at (x, y, z). B is the regional field value, and the degree of homogeneity interpreted as the structural index (SI) which is a measure of the rate of change at field distance is represented by N, and this structural index was chosen based on prior knowledge of the source geometry. Reid et al. [35], also put forward that, structural index (SI) ranges from zero (0) to three (3) for distinct bodies (N= 0 for contacts, 1 for sill/dyke/fault, 2 for pipe/horizontal bodies, and 3 for spherical bodies).

The 3D Euler deconvolution has shown to be a reliable interpretation tool for magnetic data since it requires no prior knowledge of magnetic source geometry. Another benefit of this approach is that it does not require knowledge of vector magnetisation [36]. It may thus be used in places where the causal magnetic source is buried, and the geology of the site is unknown.

3. RESULTS AND DISCUSSION

3.1 Residual Magnetic Anomaly (RMA) Map

Fig. 5 shows the RMA map, which reflects the shallow short-wavelength high-frequency anomalies after removing the regional long-wavelength low-frequency anomalies. These remaining anomalies are the focus of resource prospecting. The residual anomaly map shows different anomaly trends with a dominant NE-SW trend in most parts of the map with a predominant high-frequency anomaly having E-W trends observed between Latitude 7˚ 40´ N and Latitude 7˚ 45´ N at the western end of the map toward its centre. The exhibition of NW-SE trend by the anomalies which reflect subsurface structures is concordant with Olasehinde et al. [37] who analysed aeromagnetic data over central Nigeria's basement complex and showed that the Nigerian basement complex's structural and tectonic framework comprises NE-SW and NW-SE lineaments superimposed over a dominant N-S trend.

3.2 Residual Magnetic Anomaly Reduced to the Pole (RTP) Map

The RMA data was reduced to the pole before further processing to correct for the effect of latitude, to realign the anomalies and to have their peaks symmetrically centred over their corresponding sources because the study area is very close to the equator. This was achieved with a geomagnetic inclination of -9.45˚ and a geomagnetic declination of -2.15˚ of the central point of the study area to get the actual position of the magnetic anomalies without losing any geophysical meaning. The RTP map (Fig. 6) when compared with the RMA (Fig. 5), shows a slight variation in their magnetic.

intensities. The RTP map has a magnetic anomaly that varies from a range of -120.791 nT minimum to 76.057 nT maximum compared to the RMA map where the magnetic anomaly values within the area range from -113 nT minimum to 81.504 nT maximum.

However, the RTP map has repositioned the magnetic anomalies in comparison to the RMA map (Fig. 5), that is, portions overlain by low magnetic anomalies on the RMA map are the segments covered by high magnetic anomalies on the RTP map and vice versa. There are observed similarities between the two maps (Figs. 5 and 6) concerning the displayed anomaly in terms of anomaly trends, especially their symmetry, strike, extension, and width. The differences between the two maps are so obvious, especially the reverse in magnetic anomaly values which was higher on the RMA map and is now showing low on the RTP map.

As pointed out by Reeves [38], and Tawey et al. [1], portions (especially, the western half) on the maps (Figs. 5 and 6) having an alternating ridge and furrow-like occurrence of highs and lows anomaly are attributed to faults/highly fractured nature of the area as oxidation in fractured zones during weathering processes commonly leads to the destruction of magnetite which often allows such zones to be picked out on anomaly maps as narrow zones with markedly less magnetic variation than in the surrounding rocks.

3.3 First Vertical Derivative (FVD) map

The FVD filter (Fig. 7), has aided in revealing near-surface magnetic structures that trend NE-SW. The map showed that the area is made up of the basement and sedimentary regions with a clear boundary separating the basement and the sedimentary portions, especially around Kuroko, Oke, Mozum Okume, west of Amdi and the area around Zagi. The basement occupies the western portions while the sedimentary takes the eastern half portion of the area of study. One of the significant applications of the first vertical derivative is identifying magnetic structures [34] and it can delineate or demarcate the border between lithological units. The structural trend as observed on the FVD map (Fig. 7) is in the northeast-southwest direction, especially within the western basement portion of the study area.

Fig. 8 represents the FVD map with delineated magnetic subsurface structures overlayed on it in the black strike. From Figs. 7 and 8, sedimentary portions can be distinguished from the basement portion of the map based on the structural occurrences within those portions. Structures have been observed to occur majorly within the basement part of the study area in the western half of the study area. On overlaying the FVD structures on the RTP map (Fig. 9),

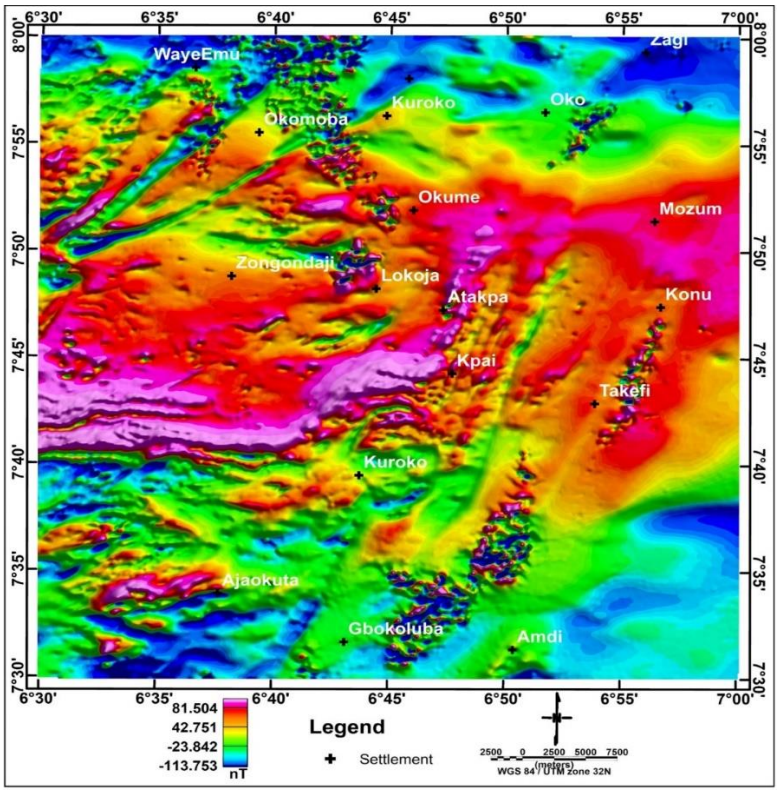

Fig. 5. Residual magnetic anomaly (RMA) map

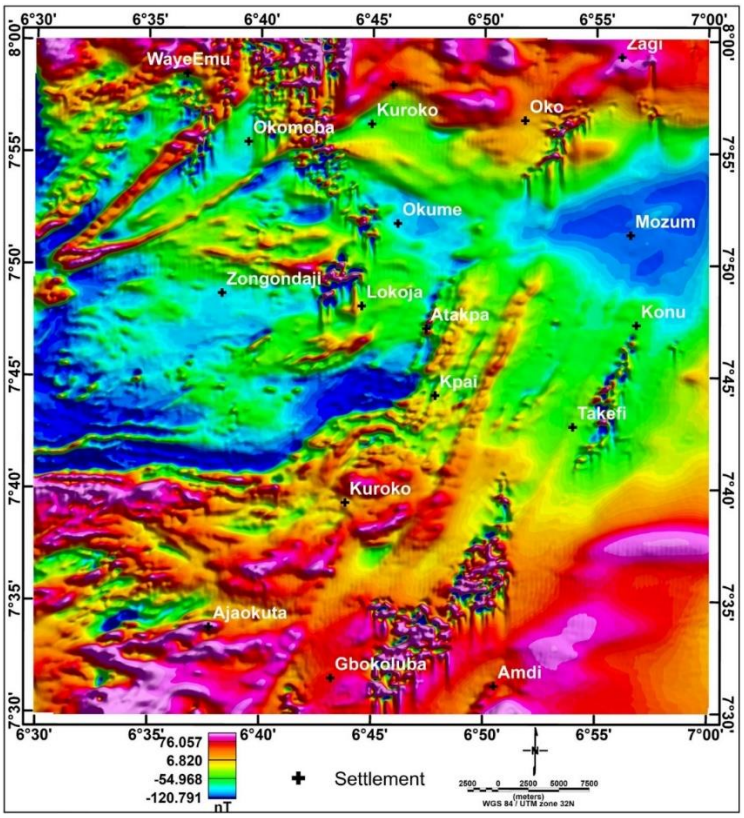

Fig. 6. Residual magnetic anomaly reduced to the pole (Map) map

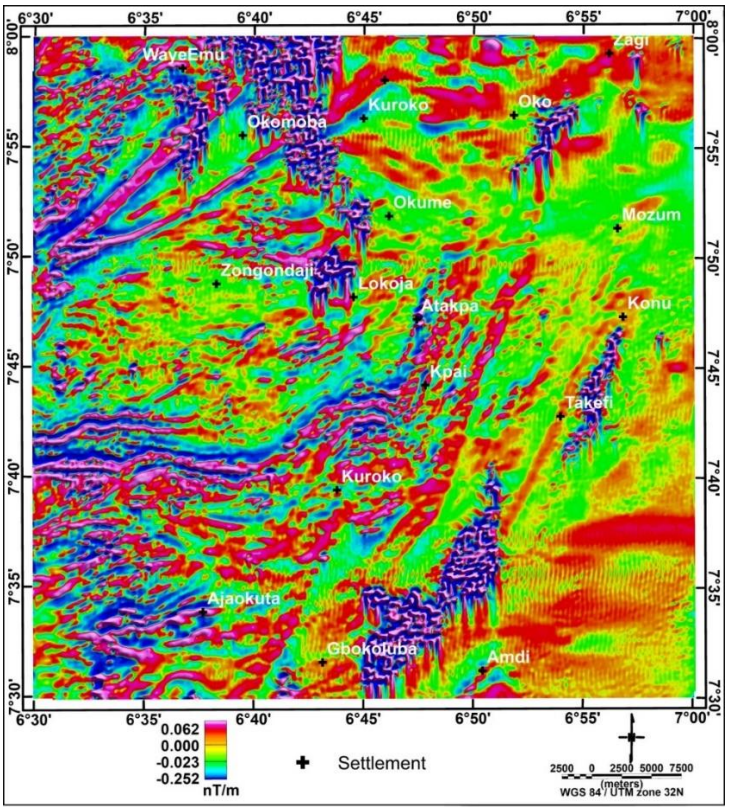

Fig. 7. First vertical derivative map of the area

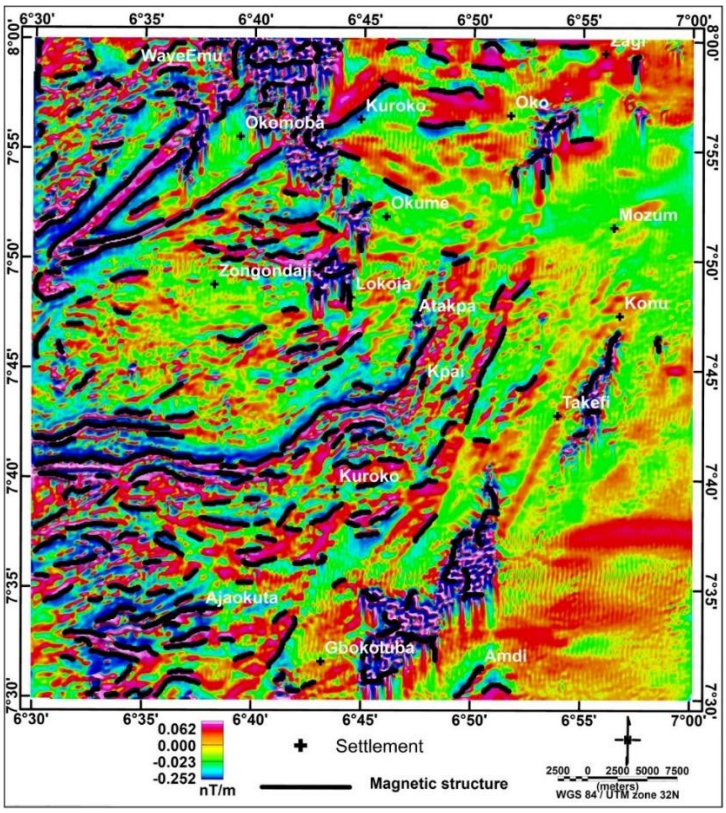

Fig. 8 First vertical derivative map of the area with structures

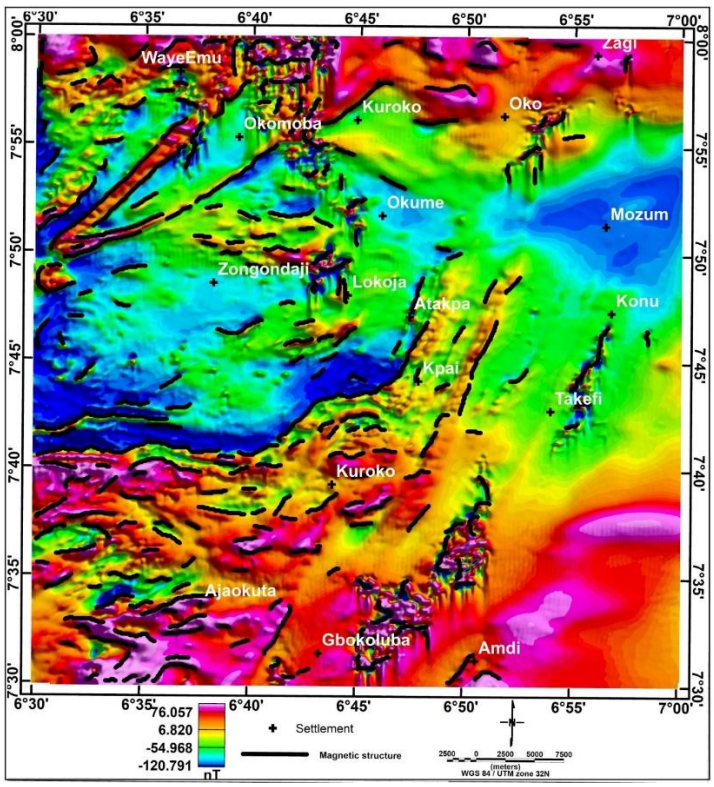

Fig. 9. RTP map overlay with FVD structures

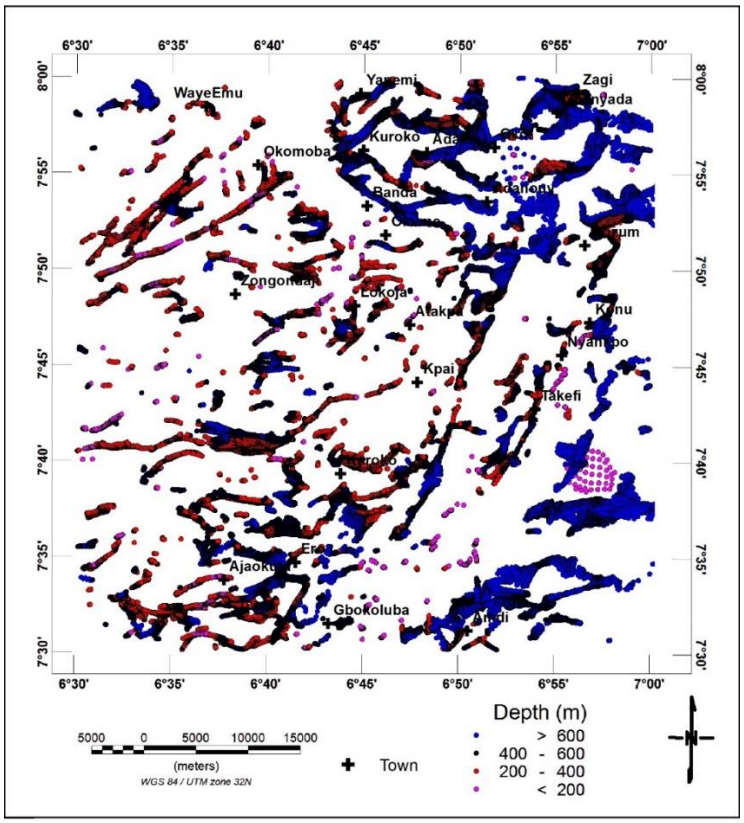

Fig. 10. 3D Euler deconvolution map with SI = 1

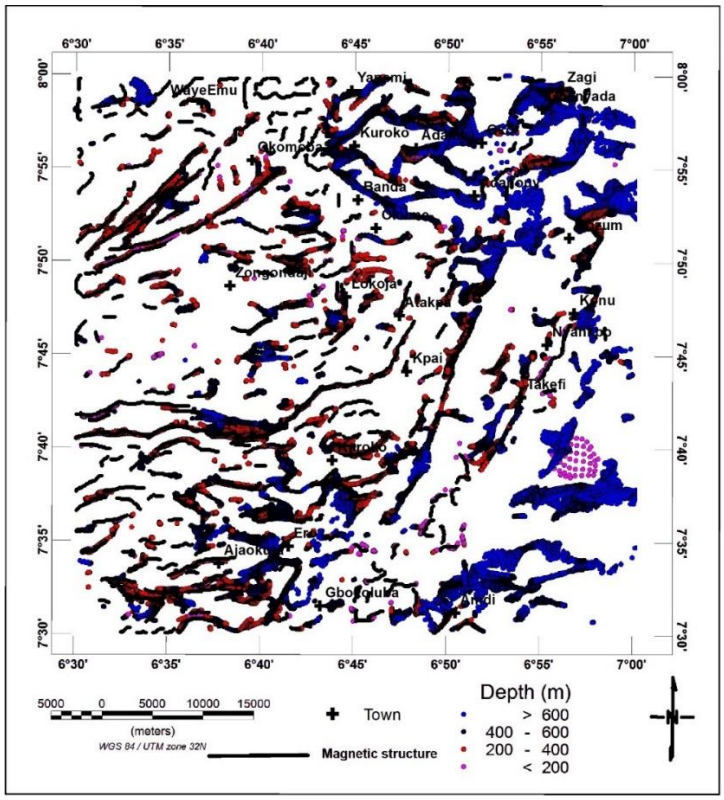

Fig. 11. 3D Euler deconvolution map with SI = 1 overlayed with FVD structures

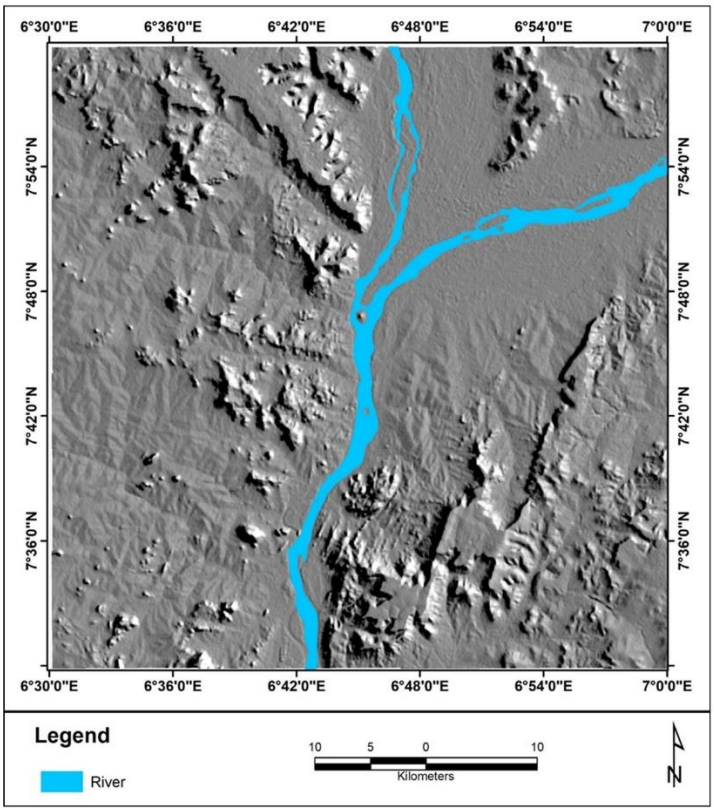

Fig. 12. Combined hillshade map of the area

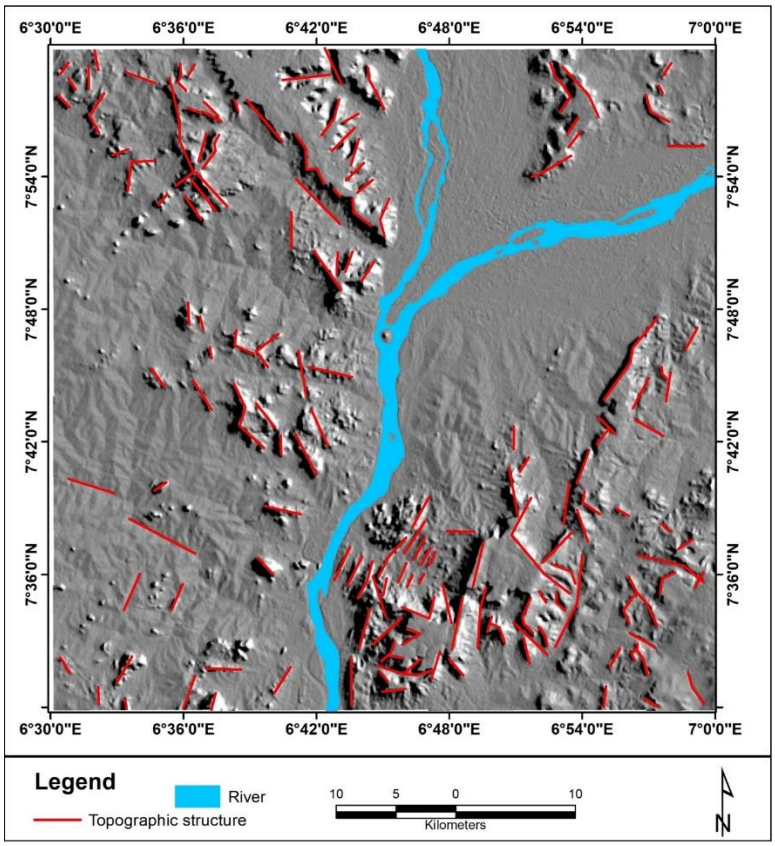

Fig. 13. Hillshade map with surface structures

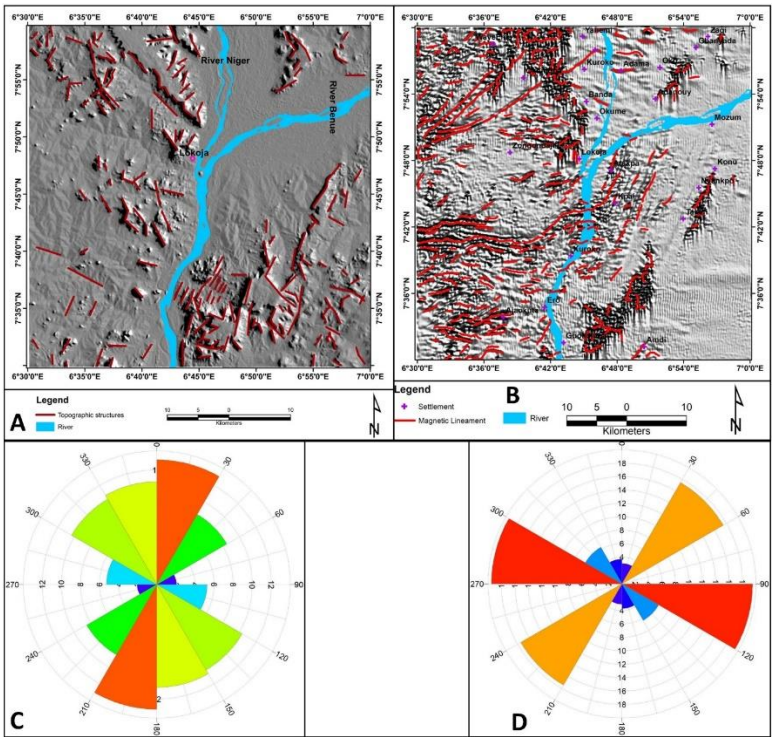

Fig. 14. a Combine Hillshade Map with Surface Structures b. Grayscale FVD Map with Structures c. Surface Structures Roses diagram and d. Subsurface Structures Rose diagram

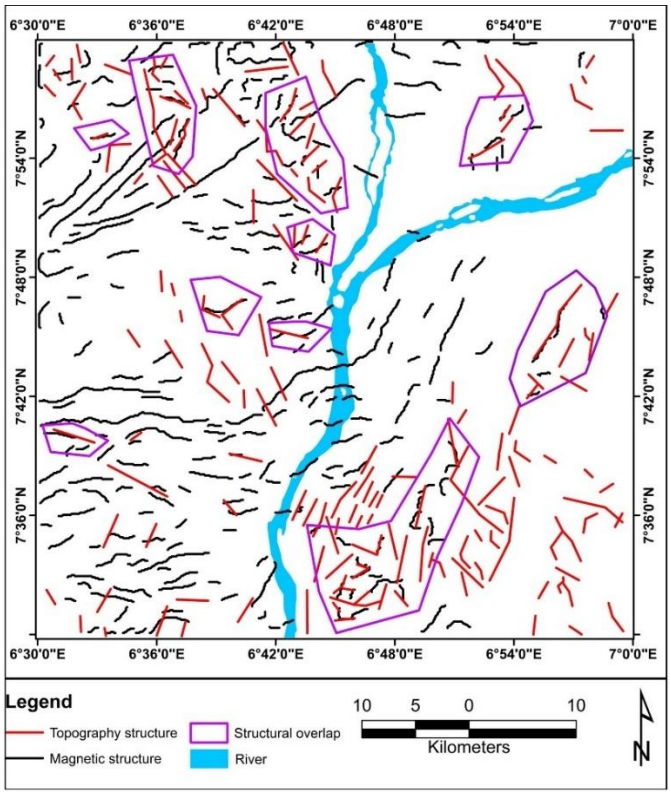

Fig. 15. Combine Surface (Topographic) Structures and Subsurface (Magnetic) Structures Showing Areas of Structural Overlap

The structures were observed to fall in place directly on the edges of the RTP anomalies within the study area especially the basement portions around Ajaokuta, directly towards the north of the area.

3.4 3D Euler Deconvolution

According to Reid et al. [35], Euler deconvolution can be used to estimate both the source boundary and its depth. The 3D Euler depth solutions for the location of the basement rock structural using the structural index of 1 for fault, represented by (Fig. 10) have been classified into four groups, those below 200 m, 200 m to 400 m, those between 400 m to 600 m and those above 600 m respectively and on the map, structures between 200 m to 400 m and 400 m - 600 m depths dominates. The 3D Euler solution map (Fig. 10) also agrees with the FVD maps (Figs. 7 and 8), as it also reveals the sedimentary and basement portion of the study area. From Fig. 10, we could infer that the basement or shallow depth to the basement occurs within the west while deeper depth to sources occurs within the west, particularly in the northeast and southeast. Also, when the structural map from the FVD was overlaid on the Euler solutions with a structural index of 1, (Fig. 11), the FVD structures coincided with the Euler structures delineated and the resultant map showed that the two methods (3D Euler deconvolution and FVD) can contribute in the delineation of the subsurface geological structures within the study area.

3.5 Hillshade and Surface structural Map of the area

Fig. 12 represents the hillshade map produced to magnify structural features within the study area while Fig. 13 represents the delineated topography or surface structures overlayed on the hillshade map. From Fig. 13, surface structures are observed to occur predominantly within the southwest, northwest, and northeastern portions of the map. The surface structures are not predominant in the basement area like the sedimentary portion of the area. on comparing Fig. 13 to Fig. 1, rocks with surface structural occurrences are undifferentiated Schist including Phyllites, banded Gneiss, Coal, sandstone, and shale (Fig. 1). Within the feldspathic sandstone and siltstone in the north,

surface structures are seen to be concentrated here.

3.6 Statistical Analysis of the Surface and Subsurface Structural Trend

Surface and subsurface structures (Figs. 14 a & b) were analysed to extract further information on the distribution and nature of the structures and for this purpose, a conventional technique called rose diagram was applied. A Rose diagram was used to display graphically different tendencies for structures like joints or fault planes representing the angular relationships of the structural lineaments. The purpose of this study is to analyse the spatial distribution of the structural lineaments extracted from combined shaded relief and aeromagnetic images according to their length and orientation to contribute to the understanding of the faults of the study area. Figs. (14 c & d) are the Roses diagram representation of the surface and subsurface structural trend of the delineated structures within the study area, by using a polar plot where the distance from the centre of the plot is proportional to the sum of the line lengths in that orientation. Structural lineament orientation or azimuth directions on the structural lineament map (Fig. 14 c & d) were measured using (Arc Map version 10.7.1) and plotted as a rose diagram using rockworks software. The Rose (azimuth-frequency) diagram (Fig. 14c) depicted that most of the surface structures extracted trends in the WNW- ESE, ENE-WSW, NE-SW, NW-SE, NNE- SSW and NNW-SSE directions. Statistical trend analysis of the surface structures using the rose diagram (Fig. 14 c) showed that the largest petal which is 26.48 % of total delineated surface structures represents structural lineaments trending in the North-North-East to South-South-West (NNE-SSW) direction. Also, 17.31% represented petal striking in the northeast-southwest (NE-SW) direction with 10.18% of the structures striking West-North-West to East-North-East (WNW-ESE) and another 20.77 % trending in the northwest-southeast (NW-SE) direction. Also, the North-North-East to South-South-West (NNE-SSW) trending structures accounted for 4.07 % while North-North-West to South-South-East (NNW-SSE) accounted for 21.18 % of the total surface or remote sensing structures within the study area.

Also, the statistical trend analysis of the subsurface structures using the rose diagram (Fig. 14 d) showed that the largest petal which is 39 % of the total delineated subsurface structures represents structural lineaments trending in the West-North-West to East-North-East (WNW-ESE) direction with 12.6 % trending in the northeast-southwest (NW-SE) direction, 7.4 % of the structures striking North-North-West to South-South-East (NNW-SSE) and another 35 % trending in the northeast-southwest (NW-SE) direction while the North-North-East to South-South-West (NNE-SSW) trending structures accounted for 6 % of the total subsurface magnetic structures within the study area.

The dominant subsurface structural trend based on the analysis is the West-North-West to East-North-East (WNW-ESE) followed by the Northeast to Southwest (NE-SW) trend. This confirmed previous structural studies assertions within the Nigerian basement complex and the adjacent Benue Trough using aeromagnetic data [21,26,39,40,37,41-45]. Also, points of structural overlap have been mapped out using a pinkish polygon (Fig. 15), which are possible points of structural continuation where fluid from the subsurface can migrate or flow freely to the surface.

4. CONCLUSION

The use of the FVD filter has aided in the identification of near-surface magnetic structures and the determination of lithological unit boundaries. The subsurface geological structures as revealed by the FVD filter are predominant within the western half of the area. The result of the 3D Euler deconvolution solution for structures and depth aligned with the FVD map result, also revealing sedimentary and basement portions with shallow depth to the basement in the west, while deeper depth to sources occurred in the northeast and southeast and this result has demonstrated that the two methods can contribute immensely in the delineation of the subsurface geological structures in the study area.

The study area hillshade map has revealed surface structures that are predominantly in the southwest, northwest, and northeastern portions of the study area. Also, the surface structures were observed to be more predominant in the sedimentary portions than in the basement parts.

The analysis of the spatial distribution of structures such as joints or faults has contributed to the understanding of the faults of the study area. Surface structures extracted trends in the

WNW-ESE, ENE-WSW, NE-SW, NW-SE, NNE-SSW, and NNW-SSE directions. The largest of them is 26.48%, representing surface structures in the NNE-SSW direction, 17.31% in the NE-SW direction, and 21.18% in the NW-SSE direction. The study found that 39% of delineated subsurface structures are structural lines in the West-North-West to East-North-East direction, with 12.6% in the northeast-southwest direction, 7.4% in the North-North-West to South-South-East direction, and 6% in the North-North-East to South-South-West direction.

The most predominant subsurface structural trend is the West-North-West to East-South-East (WNW-ESE) followed by the Northeast to southwest (NE-SW) direction. This confirmed previous structural studies assertions within the Nigerian basement complex and the adjacent Benue Trough using aeromagnetic data on dominant magnetic structural trends within this area. Also, points of structural overlap have been mapped out and these are possible points of structural continuation where fluid from the subsurface can migrate or flow freely to the surface.

COMPETING INTERESTS

Authors have declared that no competing interests exist.

REFERENCES

1. Tawey MD, Adesoji IA, Jiriko AH, Surface and subsurface lineament studies of gitata (Sheet 187) using aeromagnetic and remote sensing data 10th national water conference Benin, Edo State, Nigeria; 2021.
2. Netshithuthuni R, Sengani F, Zvarivadza T. Application of aeromagnetic, remote sensing and geological data in the delineation of the geological structures. International Journal of Georesources and Environment. 2018;4(3):141-146.
3. Olivier J, Vente JS, Jonker CZ. Thermal and chemical characteristics of hot water springs in the northern part of the Limpopo Province, South Africa. Water SA. 2011;37(4):427 - 436.
4. Maulana BR, Burhanuddin MS, Akbar MF. Lineament density and implications for the distribution of ground fissures after 2021 MW 7.3 Flores sea earthquake on Kalaotoa Island, Indonesia. Journal of Geoscience, Engineering, Environment, and Technology. 2023;8(1).
5. Rauf j, Kayambo MR, Nurjana I, Manyoe IN. Lineament extraction analysis using digital elevation model (DEM) in lahendong geothermal area, North Sulawesi. E3S Web of Conferences. 2022;400:01009.
6. Manyoe IN, Hutagalung R. Application of lineament density extraction based on digital elevation model for geological structures control analysis in suwawa geothermal area. Journal of Geoscience, Engineering, Environment, and Technology. 2022;7(3):117-133.
7. Siombonea SH, Susilob D, Maryantob S. Integration of topex satellite gravity and digital elevation model shuttle radar topography mission (DEM SRTM) imagery for subsurface structure identification at tiris geothermal area. Positron. 2022;12 (2):98-111.
8. Agbebia, Eges. Lineament analysis and inference of geological structures in bansara-boki area, Southeastern Nigeria Asian Journal of Environment & Ecology, AJEE. 2020;13(1):28-44.
9. Fajri SN, Surtiyono E, Nalendra S. Lineament analysis of digital elevation model to identification of geological structure in Northern Manna Sub-Basin, Bengkulu. IOP Conference. Series: Materials Science and Engineering. 2019; 636:012001.
10. Manjare BS, Pophare AM. Lineament mapping using shaded relief images derived from digital elevation model. Journal of Geosciences Research. 2019;4(2):155-161.
11. Akinluyi FO, Olorunfemi MO, Bayowa OG. Investigation of the influence of lineaments, lineament intersections and geology on groundwater yield in the basement complex terrain of Ondo State, Southwestern Nigeria. Applied Water Science. 2018;8:49.
12. Nugroho UC, Tjahjaningsih A. Lineament density information extraction using dem srtm data to predict the mineral potential zones. International Journal of Remote Sensing and Earth Sciences. 2016; 13(1):67-74.
13. Papadaki ES, Mertikas SP, Sarris A. Identification of lineaments with possible structural origin using ASTER images and DEM-derived products in Western crete, Greece. EARSeL eProceedings. 2011;9-26.
14. Gaafar I. Integration of geophysical and geological data for delimitation of

mineralized zones in Um Naggat area, Central Eastern Desert, Egypt. NRIAG Journal of Astronomy and Geophysics, 2015;4:86–99.
15. Telford WM, Geldart LP, Sheriff RE. Applied geophysics. Cambridge university press, second edition; 1990.
16. Murphy BS. Airborne geophysics and the Indian scenario. Journal of Indian Geophysical Union. 2007; 11(1):1–28.
17. Mohanty WK, Mandal A, Sharma SP, Gupta S, Misra S. Integrated geological and geophysical studies for delineation of chromite deposits: a case study from Tangarparha, Orissa, India. Geophysics. 2011;76:B173–B185.
18. Chaturvedi AK, Lotter C, Tripathi S, Maurya AK, Patra I, Parihar PS, Integrated application of heliborne and ground electromagnetic surveys for mapping EM conductor for uranium exploration and its subsurface validation, North Delhi Fold Belt, Rajasthan, India: A case study. Geophysics. 2013;78(1):B13–B24.
19. Patra I, Chaturvedi AK, Srivastava PK, Ramayya MS. Integrated interpretation of satellite imagery, aeromagnetic, aeroradiometric and ground exploration data sets to delineate favourable target zones for unconformity-related uranium mineralisation, Khariar Basin, Central India. Journal Geological Society India. 2013;81:299–308.
20. Gaafar IM. Geophysical mapping, geochemical evidence and mineralogy for Nuweibi rare metal albite granite, Eastern Desert, Egyptian. Open Journal of Geology. 2014;4:108–136.
21. Tawey MD, Alhassan DU, Adetona AA, Salako KA, Rafiu AA, Udesi EE. Application of aeromagnetic data to assess the structures and solid mineral potentials in part of North Central Nigeria. Journal of Geography, Environment and Earth Science International. 2020a;24(5):11-29. DOI: 10.9734/JGEESI/2020/v24i530223
22. Ayuba R, Nur A. Analysis of high-resolution aeromagnetic data and satellite imagery for mineral potential over parts of nasarawa and environs, North-Central Nigeria. International Journal of Scientific & Technology Research. 2018;7(6):103.
23. Faruwa AR, Qian W, Akinsunmade A, Akingboye AS, Dusabemariya C. Aeromagnetic and remote sensing characterization of structural elements influencing iron ore deposits and other mineralization in Kabba, southwestern Nigeria; 2021.
24. Ogunmola JK, Gajere EN, Ayolabi EA. Olobaniyi SB, Jeb DN, Agene IJ. Structural study of wamba and environs, north-central Nigeria using aeromagnetic data and Nigeria Sat-X image. Journal of African Earth Sciences. 2015;111:307-321. Available:https://doi.org/10.1016/j.jafrearsci.2015.07.028
25. Ebele JE, Nur A. Regional groundwater studies using high-resolution aeromagnetic data in Abuja and environs, North-Central Nigeria. Applied Journal of Physical Science. 2020;2(3):68-79.
26. Tawey MD, Alhassan DU, Adetona AA, Salako KA, Rafiu AA, Udesi EE. Edge detection and depth to magnetic source. Estimation in Part of Central Nigeria. Physical Science International Journal. 2020b;24(7):54-67. DOI: 10.9734/JGEESI/2020/v24i530223
27. NGSA. Geology and Structural Lineament Map of Nigeria; 2006.
28. Yaoguo L, Douglas WO. Stable reduction to the pole at the magnetic equator. Geophysics, 2001;66(2):571-578.
29. Baranov V. A new method of interpretation of aeromagnetic maps: Pseudogravimetric anomalies. Geophysics. 1957;22:259-283.
30. Bhattacharyya BK. Two-dimensional harmonic analysis as a tool for magnetic interpretation. Geophysics. 1965;30:829-857.
31. Li X. Magnetic reduction-to-the-pole at low latitudes. Observations and considerations. The Leading Edge. 2008;27(8):961-1080. Available:https://doi.org/10.1190/1.2967550
32. Milligan PR, Gunn PJ. Enhancement and presentation of airborne geophysical data. AGSO Journal of Australian Geology and Geophysics. 1997;17(2):64-774.
33. Luo Y, Xue DJ, Wang M. Reduction to the pole at the geomagnetic equator. Chinese Journal of Geophysics. 2010;53(6):1082-1089.
34. Foss C. Magnetic data enhancement and depth estimation. In H. Gupta (Ed.), Encyclopedia of Earth Sciences Series. 2011;736-746.
35. Reid AB, Allsop JM, Granser H, Millet AJ, Somerton IW. Magnetic interpretation in three dimensions using Euler deconvolution. Geophysics. 1990;55: 80-91.

36. Thompson DT. EULDPH: A new technique for making computer-assisted depth estimates from magnetic data. Geophysics. 1982;47:31-37.
37. Olasehinde PI, Pal PC, Annor AE. Aeromagnetic anomalies and structural lineament in the Nigerian basement complex. Journal of African Earth Sciences. 1990;11(3/4):351-355.
38. Reeves C. Aeromagnetic surveys, principle practice and interpretation. Geosoft E-Publication; 2005.
Available:www.geosoft.com/media/uploads/resources/technical/aeromagnetic_survey_Reeeves.pdf
39. Tawey MD, Ehinlaiye AO, Odia-Oseghal JO. Surface and subsurface structural mapping via airborne magnetic and remote sensing data: A study of kachia (Sheet 166), North-Central Nigeria. African Journal of Environmental Sciences & Renewable Energy. 2023b;12(1);1-17.
40. Andrew J, Alkali A, Salako KA, Udensi EE. Delineating mineralisation zones within the Keffi-Abuja area using aeromagnetic data. Journal of Geography, Environment and Earth Science International. 2018;15(3):1-12.
ISSN: 2454-7352
DOI: 10.9734/JGEESI/2018/370
41. Ajakaiye DE, Hall DH, Miller TW, Verherjen PJT, Awad MB, Ojo SB. Aeromagnetic anomalies and tectonic trends in and around the Benue Trough Nigeria. Nature. 1986;319:582-584.
42. Gaafar IM. Geophysical signature of the vein-type uranium mineralisation of Wadi Eishimbai, Southern Eastern Desert, Egypt. Arabian Journal of Geoscience. 2012;5:1185–1197.
43. Obaje NG. Geology and mineral resources of Nigeria. Berlin: Springer-Verlag, Heidelberg; 2009.
44. Sabins FF. Remote sensing: Principles and interpretation. W.H. Freeman and Company, New York. 1997;361.
45. Wright JB. Geology and Mineral Resources of West Africa; 1985.

Peer-review history:
The peer review history for this paper can be accessed here:
https://www.sdiarticle5.com/review-history/114757